

## Accepted Manuscript

Title: Synthesis and characterization of well dispersed nickel-incorporated SBA-15 and its high activity in syngas methanation reaction

Author: Miao Tao Xin Meng Zhong Xin Zhicheng Bian  
Yuhao Lv Jia Gu



PII: S0926-860X(16)30085-0  
DOI: <http://dx.doi.org/doi:10.1016/j.apcata.2016.02.019>  
Reference: APCATA 15778

To appear in: *Applied Catalysis A: General*

Received date: 19-11-2015  
Revised date: 10-2-2016  
Accepted date: 15-2-2016

Please cite this article as: Miao Tao, Xin Meng, Zhong Xin, Zhicheng Bian, Yuhao Lv, Jia Gu, Synthesis and characterization of well dispersed nickel-incorporated SBA-15 and its high activity in syngas methanation reaction, Applied Catalysis A, General <http://dx.doi.org/10.1016/j.apcata.2016.02.019>

This is a PDF file of an unedited manuscript that has been accepted for publication. As a service to our customers we are providing this early version of the manuscript. The manuscript will undergo copyediting, typesetting, and review of the resulting proof before it is published in its final form. Please note that during the production process errors may be discovered which could affect the content, and all legal disclaimers that apply to the journal pertain.

## Synthesis and characterization of well dispersed nickel-incorporated SBA-15 and its high activity in syngas methanation reaction

Miao Tao<sup>1</sup>, Xin Meng<sup>1,2</sup>, Zhong Xin<sup>1,2\*</sup>, Zhicheng Bian<sup>1</sup>, Yuhao Lv<sup>1</sup>, and Jia Gu<sup>1</sup>

<sup>1</sup>Shanghai Key Laboratory of Multiphase Materials Chemical Engineering, <sup>2</sup>State Key Laboratory of Chemical Engineering, School of Chemical Engineering, East China University of Science and Technology, Shanghai, People's Republic of China

### \*Information for Corresponding author

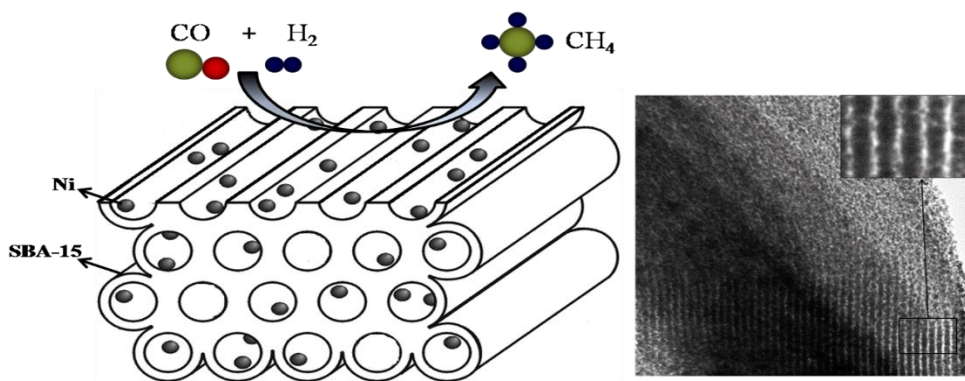
Name: Zhong Xin

E-mail address: xzh@ecust.edu.cn(Z.Xin).

Tel: +86-021-64251005; Fax: +86-021-64240862

Address: Mailbox 545, East China University of Science and Technology, No. 130, Meilong Road, Shanghai, 200237.

### Graphical abstract



### Highlights:

- An original nickel-incorporated catalyst was synthesized by the pH-adjusting method.
- The Ni-S15 catalyst showed high activity with 98% CH<sub>4</sub> yield in CO methanation.
- This catalyst can be used in the production of SNG from coal or dry biomass.

**Abstract:**

Ni-incorporated SBA-15 materials were successfully synthesized by pH adjusting method using sodium hydroxide (NaOH) as the pH regulator and tetraethyl orthosilicate (TEOS) as the silica source. The results of transmission electron microscope (TEM) and H<sub>2</sub> pulse chemisorption showed that nickel particles of the Ni-S15 catalysts prepared by pH adjusting method were much finer and more uniform dispersion than those of Ni/S15 catalyst prepared by traditional impregnation method. The nickel dispersions of Ni-S15(pH8) and Ni/S15 were 3.6% and 2.5%, respectively. In addition, the pH value strongly affected the amount of nickel introduced in the silica framework. The catalytic performances were also investigated for synthetic natural gas (SNG) production via syngas methanation reaction. The Ni-S15(pH8) catalyst prepared by pH adjusting method achieved the best activity with 100% CO conversion and 98.6% CH<sub>4</sub> yield at 350°C, 0.3MPa and 15000mL/g/h. Meanwhile, the Ni-S15(pH8) catalyst possessed excellent stability and high-temperature-resistant performance due to the strong interaction between NiO and support.

**Keywords:** nickel-incorporated SBA-15; pH-adjusting; improved dispersion; syngas methanation

**1. Introduction**

Among different forms of fossil fuels, natural gas is ideal owing to its ready availability, high energy density and conversion efficiency [1]. In recent years, due to the rise of the natural gas price, synthetic natural gas (SNG) production from coal has attracted increasing attention [2]. Coal is firstly converted into syngas through the processes of gasification, water-gas shift and cleaning [3]. Then syngas reacts in a fixed-bed reactor in the presence of a catalyst to produce CH<sub>4</sub>. The methanation

process is highly exothermic and is shown as follows:  $\text{CO} + 3\text{H}_2 = \text{CH}_4 + \text{H}_2\text{O}$ ,  $\Delta H_{298\text{K}} = -206.1\text{kJ/mol}$  [4]. The catalyst is considered unanimously as a key factor in the production of methane. Ni-based  $\text{Al}_2\text{O}_3$  is the most widely used catalyst to produce methane [5, 6]. However, low metal dispersion and nickel sintering during methanation reaction limited the wide application of Ni/ $\text{Al}_2\text{O}_3$  catalyst [7, 8]. Therefore, it is still a challenge to develop methanation catalysts with good metal dispersion and superior heat-resistance.

In addition, the chemical and texture properties of the support usually affect the metal-support interaction and metal dispersion, which further influence the reactant conversion and product selectivity [9, 10]. Mesoporous silicas have attracted increasing attentions due to the large surface area and uniform mesoporous channels since the researchers at Mobil Corporation reported M41S in the early 1990s. In our previous work [11], the nickel based MCM-41 catalyst prepared by impregnation method showed good catalytic performance in the CO methanation, but poor thermal stability, which was easily sintered after calcined at high temperature. We also found that the nickel incorporated MCM-41 catalyst prepared by a hydrothermal synthesis method showed good performance in the heat resistant test, and yet the mesoporous structures of the catalysts gradually be destroyed when the Ni content was higher than 10wt% [12]. SBA-15 [13], another version of the structured silica materials, has a broader application in catalysis [14-16] because of its higher surface area, larger pore size, thicker pore wall, higher thermal and hydrothermal stabilities than MCM-41 materials. There is also no acidic site on the surface, which inhibits the formation of carbon deposition. What's more, there are silanol groups on the silica surface which influence the interaction between metal and support [17]. There are extensive literatures [18-20] reported that the catalysts using SBA-15 as the support had improved dispersion of active metals, higher effective diffusion

coefficient and catalytic performance.

However, it is very difficult to prepare SBA-15 containing heteroatoms in the framework because of the strong acidic synthesis condition ( $\text{pH} < 1$ ). Metals always exist in cationic form rather than oxo species under acidic condition and they therefore cannot be introduced into the framework of SBA-15. Many efforts have been devoted to the study on the incorporating of Al [21], Ti [22], Fe [23], Co [24] and Sn [25] into the SBA-15 framework. Wu et al [26] reported that the  $\text{Al}^{3+}$  and  $\text{Ti}^{4+}$  could be largely introduced into SBA-15 mesoporous molecular sieves by “pH-adjusting” method for the first time. Cui and coworkers [27] synthesized cobalt-substituted SBA-15 by a simple and effective method designated as “pH-adjusting” and demonstrated that most of cobalt species were in the single-site  $\text{Co(II)}$  state. They also found that the catalyst exhibited much higher activity than Co-MCM-41 and Co/SBA-15 in the epoxidation of styrene with  $\text{O}_2$ .

So far, however, few reports [28] were presented to demonstrate the incorporation of Ni into the SBA-15 silica framework. The effect of pH value on the physicochemical properties and catalytic performance were also unknown. In this work, several Ni incorporated SBA-15 catalysts were prepared by direct synthesis. Sodium hydroxide was used to adjust the pH of synthesis gels by taking advantage of the pH control and the salt addition simultaneously. All catalysts were evaluated in syngas methanation reaction. The physicochemical properties of the catalysts were also characterized by X-ray diffraction (XRD),  $\text{N}_2$  adsorption-desorption,  $\text{H}_2$ -temperature programmed reduction ( $\text{H}_2$ -TPR), inductively coupled plasma (ICP) elemental analysis,  $\text{H}_2$  pulse chemisorptions, scanning electron microscope (SEM) and transmission electron microscopy (TEM).

## 2. Experimental

### 2.1 Preparation of catalysts

All chemicals used were analytical grade, including poly (ethylene glycol) -block- poly (propylene glycol) -block- poly (ethylene glycol) EO<sub>20</sub>PO<sub>70</sub>EO<sub>20</sub> (P123, Aldrich), tetraethyl orthosilicate (TEOS), hydrochloric acid of concentration 36%-38%, nickel(II) nitrate hexahydrate (Ni(NO<sub>3</sub>)<sub>2</sub> • 6H<sub>2</sub>O), sodium hydroxide (NaOH) and deionized water.

The nickel-incorporated SBA-15 was prepared by the pH-adjusting method. The molar ratio of TEOS, P123, HCl and H<sub>2</sub>O is 1, 0.017, 5.88 and 136. The detailed synthesis route [29] was as follows: 4.0g P123 triblock copolymer surfactant was dissolved in 2.4M HCl solution at 40°C to obtain a clear solution. Subsequently, TEOS was gradually added to the solution and stirred for 4h. Then 1.3g Ni(NO<sub>3</sub>)<sub>2</sub> • 6H<sub>2</sub>O was added to the mixture, followed by additional stirring at 40°C for 20h. The resulting gel was transferred into an autoclave and crystallized statically at 110°C for 24h. After the procedure above, the pH of the system was adjusted to a certain value by adding sodium hydroxide aqueous solution dropwise at room temperature and the mixture was crystallized again at 110°C for another 24h. After being cooled to room temperature, the product was isolated by filtering, washing with water and drying at 80°C overnight. Finally, the sample was calcined under air at 550°C for 6h (heating ramp 1°C/min) to remove the surfactant. The obtained product is denoted as Ni-S15(pHx), where x standing for 6, 7 and 8. On the contrary, Ni/S15 was prepared by the traditional impregnation method and used as a reference.

## 2.2 Characterizations

The textural properties of the catalysts were derived from N<sub>2</sub> adsorption/desorption measurement using an ASAP 2000 (Micromeritics) instrument. The pore size distribution was calculated by the Barret-Joyner-Hallender (BJH) method using the desorption branch. The specific surface area was calculated according to the Brunauer-Emmett-Teller (BET) method during the

relative pressure ( $p/p_0$ ) range of 0.1-0.3. Prior to the test, the sample was degassed to 300°C for 4h under vacuum. Nickel content in each sample was analyzed with inductively coupled plasma-atomic emission spectroscopy (ICP-AES) on TJA Atomscan 16 spectrometer. X-ray diffraction (XRD) was used to investigate the structure of catalysts and the crystalline phases of the Ni particles on the catalysts. The XRD patterns were obtained with a Bruker D8 Advance X-ray diffractometer using Ni-filtered Cu radiation at 3kW. The small and wide angle scan ranges were 0.5°-5° and 10°-80° with 0.02° steps, respectively. The reduction behavior of the catalysts was investigated by H<sub>2</sub>-temperature-programmed reduction (H<sub>2</sub>-TPR), and the TPR profiles were measured by Micromeritics AutoChem II 2920 adsorption instrument. Prior to H<sub>2</sub>-TPR measurement, the sample was purged with high purity Ar at a flow rate of 30mL/min at 150°C for 2h before cooling down to 50°C. A stream of Ar containing 10% H<sub>2</sub> at a flow rate of 30mL/min was then switched to the catalyst while the temperature was increased at a rate of 10°C/min to 800°C. H<sub>2</sub> pulse chemisorption (Micromeritics AutoChem II 2920) was carried out at 40°C to investigate the dispersion and metallic surface area of nickel metal in the reduced catalyst. First, the catalyst sample was reduced in a fixed-bed reactor by H<sub>2</sub> (50mL/min) for 2h at a certain temperature and cooled to room temperature in N<sub>2</sub> atmosphere. Then 0.05g sample was filled in the quartz tube and pretreated in He for 1h at 200°C to remove the impurities and adsorbed hydrogen. After cooling to room temperature in Ar, 10%H<sub>2</sub>/Ar pulse adsorption was performed at 40°C for 10 times. Transmission electron microscope (TEM) images of the samples were obtained with a JEOL-2010 instrument. TEM-EDS analyses was conducted to examine the composition of the samples. The samples were prepared by directly suspending the powder in ethanol with ultrasonication. A copper microscope grid covered with perforated carbon was dipped into the suspension for observation.

## 2.3 Catalytic performances tests

Syngas to methane reaction was conducted in a fixed-bed stainless steel reactor with an inner diameter of 10mm. To prevent hot spot formation in the process, the sample was diluted with quartz sand (3g, 50-80mesh). Before the reaction, the catalyst (0.5g, powder, sieve fraction 100 mesh) was reduced by high purity H<sub>2</sub> with 50mL/min at a certain temperature for 2h. Subsequently, the reactor was cooled down to 300 °C before the gas flow (H<sub>2</sub>) was switched to syngas (H<sub>2</sub>/CO=3, WHSV=15000ml/g/h) and the pressure was increased to 0.3MPa. The outlet gases were analyzed by an on-line gas chromatograph (Techcomp, GC7890T). A thermal conductivity detector (TCD) and flame ionization detector (FID) were used to analyze gaseous products (CO, CO<sub>2</sub> and CH<sub>4</sub>). The equations used for calculating the CO conversion and CH<sub>4</sub> yield are shown below:

$$\text{Conversion of CO(\%)} = \frac{\text{moles of CO reacted}}{\text{moles of CO supplied}} \times 100 \quad (1)$$

$$\text{Yield of CH}_4(\%) = \frac{\text{moles of CH}_4 \text{ formed}}{\text{moles of CO supplied}} \times 100 \quad (2)$$

## 3. Results and discussion

### 3.1 Physicochemical properties of catalysts

#### 3.1.1 Effect of pH value on the textural properties

The textural properties of pure silica SBA-15 and fresh Ni-S15(pH<sub>x</sub>) (x=6, 7, 8) catalysts were characterized by N<sub>2</sub> adsorption-desorption measurement. Combined with the results of Fig.S1, it suggested that the pH-adjusting method was effective in maintaining the highly ordered mesostructure of the catalysts even under high pH conditions. Besides, the order of 2D-hexagonal P6mm structure of Ni-S15 samples decreased as the pH increased. Corresponding textural properties of all the samples were summarized in Tab.1. Compared with pure silica SBA-15, the introduction of nickel made the surface area significantly decrease. Meanwhile, with the increasing of pH value, the

surface area gradually decreased. It was proposed that some of nickel species was incorporated into mesoporous channels. On the other hand, pore diameter had an obvious increase when nickel was introduced into the molecular sieves, and the parameter became larger with pH value rising. It might be because of the longer bond length of Ni with oxygen than that of Si-O [30]. As pH value increased, more nickel ions introduced into the framework of the mesoporous silica, which made pore diameter further increase. For Ni/S15 catalyst, the BET surface area decreased and the average pore size increased after addition of nickel, indicating the pore blockage by the introduced nickel [31, 32].

### 3.1.2 Crystalline structures

The crystalline structures of the fresh catalysts and the sizes of the Ni particles on the catalysts were determined using XRD. The results were shown in Fig.1. For all the catalysts, the diffraction peaks at about  $1^\circ$  on the small angle XRD patterns implied that the catalysts retained the ordered hexagonal mesoporous structures of SBA-15 [33]. Moreover, the samples synthesized by pH-adjusting method showed multiple well-resolved peaks. This indicated that the structural order of Ni-S15 catalysts was higher than that of Ni/S15. In this block copolymer template system, it has been well-documented that ordered structure of the mesoporous materials can be improved by the addition of salts into the synthesis gels [34]. The presence of salt in the synthesis gel was proposed to decrease the critical micelle concentration and therefore to facilitate the arrangement of the mesostructures [35]. In our study, the produced NaCl was responsible for effectively improving the ordered structure since sodium hydroxide was used to adjust pH during the synthesis. However, further increased of pH negatively affected the structure of the samples, which was in agreement with the results of Lou et al [24]. The mesoporous silica synthesized under acidic condition had an

electrically neutral framework. Under weakly alkaline conditions, hydrolysis tend to speed up due to the presence of  $\text{OH}^-$ . On the other hand, although lower pH was favorable to highly ordered mesostructure, it resulted in lower amount of nickel introduction. For instance, when pH was 8, 8.4 wt% of nickel was introduced into the mesoporous molecular sieves for Ni-S15(pH8), whereas there was only 1.7 wt% of nickel content if pH decreased to 6, confirmed by ICP-AES analysis shown in Table 1. An obvious phenomenon was that the amount of nickel species incorporated into the SBA-15 increased with the increase of pH value. It was due to the formation of  $\text{Ni}(\text{OH})_2$  precipitation which held the  $\text{Ni}^{2+}$  incorporating into the framework of support.

In the wide angle XRD patterns (Fig.1B), the wide and broad peaks at  $10\text{-}30^\circ$  were ascribed to amorphous silica. The pattern of Ni/S15 catalyst prepared with impregnation method showed the characteristic diffraction peaks of the NiO particles ( $2\theta=37.2^\circ$ ,  $43.2^\circ$  and  $62.8^\circ$ ) [36]. However, there was no obviously characteristic diffraction peaks of NiO particles in the curve of Ni-S15(pH6) catalyst. It could be due to the low nickel content. With the increase of pH value, the diffraction peaks intensity of nickel species increased, which suggested the particle size and content of nickel increasing. It was in line with the results of ICP-AES analysis. It was generally known that the particle sizes increased with the increasing metal content, so the particle size increased with the increase of pH value. Even so, the increasing nickel surface area was obtained. But it was unable to calculate the NiO particle size due to its diffusion distribution. Compared with the Ni/S15 catalyst, it could be found that the NiO particles of the Ni-S15 catalysts were much finer and more uniform dispersion. It was also proved by the results of  $\text{H}_2$  pulse chemisorption (seen in Tab.1). Although the nickel content of Ni/S15 (9.8%) was larger than that of Ni-S15(pH8) (8.4%), the nickel surface area was smaller. This showed that the increase of nickel content was not enough to offset the adverse

effect of increasing metal particle size.

### 3.1.3 Morphologies and metal distributions

The morphologies of SBA-15 and the distributions of Ni particles over the catalysts were further investigated by SEM and TEM, and the results were shown in Fig.2. Figure (A) showed the SEM image of SBA-15, it could be seen that the SBA-15 possessed very long rod-shaped material. The TEM image (Fig.2B) showed the highly ordered one-dimensional channels of SBA-15. Besides, ordered mesoporous structures of SBA-15 could be observed on the TEM images of all the catalysts, which were consistent with the results of BET and XRD. It was observed that more uniform distributions and smaller particles of the Ni species formed in the Ni-S15 catalysts compared with that in the Ni/S15 catalyst. The amount of nickel particles increased with the increase of pH value, which was in accordance with the results of ICP-AES analysis. It could be speculated that using pH adjusting method could decrease the nickel particle sizes over SBA-15 from the results of XRD and TEM.

TEM-EDS technology was carried out to demonstrate the incorporation of nickel species into the SBA-15 more clearly. The curves (Fig.2) proved once again the co-existence of nickel, silicon and oxygen elements in the samples. The peaks of Cu and C could be ascribed to the elements in the copper microscope grid covered with perforated carbon. In addition, the co-assembly of metal hydrate and TEOS had been proved under the direction of surfactant [37, 38]. When the alkali (NaOH) was added to adjust the pH value, the metal hydrate would react with  $\text{OH}^-$  forming  $\text{Ni}(\text{OH})_2$  precipitation, which led to the incorporation of metal species into the framework of the support. For better understanding the synthesis procedure, a schematic diagram was shown in Fig.3.

### 3.1.4 Effect of pH value on the metal-support interactions

The reduction behaviors of NiO and the interactions between Ni particles and supports were characterized by H<sub>2</sub>-temperature programmed reduction (H<sub>2</sub>-TPR) method, and the results were shown in Fig.4. According to the reduction temperature, the reducible NiO were classified into three types: I-type, II-type and III-type NiO species. Generally, the reduction temperature of NiO reflected the interaction between NiO and support [39]. The I-type NiO species were ascribed to free nickel oxides possessing a weak interaction with the support, the II-type NiO species had a moderate interaction with the support, and the III-type NiO species had the strongest interaction with the support which were the most difficult to reduce. The TPR quantitative results of the catalysts were listed in Tab.2.

It could be seen that there were three reduction peaks of NiO on the TPR profiles of all the catalysts prepared by pH-adjusting method. However, there were just I-type and II-type NiO species for Ni/S15 catalyst, which suggested that the interaction between NiO and support was relatively weak. For Ni-S15 catalysts, the fraction of III-type NiO species increased and I-type NiO species decreased with the increase of pH value. It was probably due to that the excess OH<sup>-</sup> would react with Ni<sup>2+</sup> forming Ni(OH)<sub>2</sub> precipitation, which held the Ni<sup>2+</sup> incorporating into the framework of SBA-15. The amount of Ni species incorporated into the siliceous framework of Ni-S15 increased along with the increase of pH value, which led to the stronger interaction between NiO and support. The agglomeration of nickel particles became more difficult with the enhancement of interaction between NiO and support, which resulting in the better anti-high-temperature performance of the catalyst. It could be confirmed by the results of the heat-resistant performance test.

### 3.2 Catalytic performance of catalysts in CO methanation

#### 3.2.1 Effect of reaction temperature and pH value on the activities of catalysts

Generally, the reaction temperature had great influence on catalytic performance. The influences of reaction temperature on the CO conversion and CH<sub>4</sub> yield over Ni-S15 and Ni/S15 catalysts were presented in Fig.5. The carbon balance values were about 99% on the average. As illustrated in Figure S2 and Table S1, the nickel dispersion and metallic surface area obtained the maximum, which resulted in the best catalytic activity when the reduction temperature was 600°C. Therefore, all the catalysts were first reduced by H<sub>2</sub> (50mL/min) at 600°C. The CO conversion and CH<sub>4</sub> yield over Ni-S15(pH6) increased quickly with the increasing of reaction temperature at first. For example, CH<sub>4</sub> yield was 0% at 300°C, quickly rose to 35.8% at 350°C, and to 62.6% at 400°C. The CO conversion of Ni-S15(pH8) and Ni/S15 catalysts maintained 100% in the range of 300-450°C. The yield of CH<sub>4</sub> over all catalysts first increased and then decreased as the reaction temperature increased. It was due to thermodynamic limitation. For the Ni-S15(pH6), Ni-S15(pH7) and Ni-S15(pH8) catalysts, the highest CH<sub>4</sub> yield was 73.9%, 96.0% and 98.6%, respectively. This further confirmed that lower pH led to the introduction of less nickel into the molecular sieves which brought about lower activity. In addition, the highest CH<sub>4</sub> yield of the Ni/S15 catalyst was only 76.2%. It was clear that pH-adjusting method could significantly improve the catalytic activity of the Ni-based catalysts in the CO methanation reaction. The activity of nickel based catalyst depended on the number of active sites located on the surface. According to the results of H<sub>2</sub> pulse chemisorption, the metal dispersions of Ni-S15(pH8) and Ni/S15 were 3.6% and 2.5%, respectively. The Ni-S15(pH8) catalyst had better dispersion of nickel particles which resulted in higher catalytic activity than Ni/S15 catalyst.

During methanation, some side-reactions may occur which affects the CH<sub>4</sub> selectivity and CH<sub>4</sub>

yield. Besides the syngas methanation reaction ( $\text{CO} + \text{H}_2 = \text{CH}_4 + \text{H}_2\text{O}$ ), water-gas shift reaction ( $\text{CO} + \text{H}_2\text{O} = \text{CO}_2 + \text{H}_2$ ) can also occur. In addition, the carbon monoxide disproportionation reaction ( $2\text{CO} = \text{C} + \text{CO}_2$ ) is important since carbon on the catalyst surface is considered as a necessary intermediate during the methanation reaction [40]. The carbon balance values were about 99% on the average by calculating the sums of unreacted carbon monoxide, carbon dioxide and methane in the product. Therefore, the main by-product is carbon dioxide in the syngas methanation process.

### 3.2.2 Heat-resistant performance

CO methanation reaction is a strongly exothermic reaction [41] and the heat released in the process of the reaction may easily lead to the catalyst sintering and the loss of the catalyst activity. Thus, the catalytic stability of the catalyst after high temperature calcination plays a vital role in the industry. The activities of the catalysts were tested at  $400^\circ\text{C}$  under 0.3MPa with a WHSV of 15000 ml/g/h, after that the catalysts were calcined at  $700^\circ\text{C}$  for 2h under 0.3MPa in reactant gases ( $n(\text{H}_2):n(\text{CO}) = 3:1$ , 15000 ml/g/h), and then cooled to  $400^\circ\text{C}$  for the activity evaluation under the same conditions. The high-temperature resistance performance of the catalysts were evaluated through comparing the activities of catalysts before and after calcination, and the catalytic activities of the catalysts before and after calcination were shown in Tab.3.

For all the Ni-based catalysts except Ni-S15(pH8), there were significant declines of catalytic activities after calcination at  $700^\circ\text{C}$  for 2h in reactant gases. The  $\text{CH}_4$  yields of Ni-S15(pH6), Ni-S15(pH7) and Ni/S15 decreased by 37.5%, 16.9% and 40.0%, respectively. In order to investigate the main factor in the decrease of catalytic activities,  $\text{N}_2$  adsorption-desorption and  $\text{H}_2$  pulse chemisorption analysis were carried out. The results were shown in Tab.1. The BET surface areas of all the catalysts were dropped by 20-25% and the average pore sizes barely changed. This was due to

the partial collapse of the pore structure. It was also noticeable that the descending degree of all the catalysts were lower than that of SBA-15 (~47%), showing that the incorporation of Ni in SBA-15 had the effect in protecting the pore structures from collapse upon calcination. The similar phenomenon was also observed in the paper of Shih-Yuan Chen [42]. The metal dispersions of Ni-S15(pH6), Ni-S15(pH7) and Ni/S15 catalysts dropped 0.9%, 0.6% and 1.1%, respectively. However, the metal dispersion of Ni-S15(pH8) remained unchanged. It was suggested that the main reason for the decline of activities during calcination in reactant gases was the nickel particles sintering, not the structure change of support. In addition, the high-temperature-resistant performance of Ni-S15 catalysts became better with the increase of pH value. It was because using pH-adjusting method could strengthen the interactions between NiO and support based on the TPR results. At the same time, the fraction of III-type NiO species increased with the increase of pH value. Thus, Ni-S15(pH8) catalyst showed the best high-temperature-resistant performance with excellent catalytic activity.

Considering the 100% conversion of CO at 400°C, the excellent methanation behavior of Ni-S15(pH8) after the calcination step might be caused by its pristine methanation activity. In order to better understand the phenomenon, the heat-resistant performance was repeated at 250°C. The thermodynamic equilibrium was not achieved under this thermal condition. The results were listed in Tab.3 and the same trend were obtained. The CO conversions of Ni-S15(pH6) and Ni-S15(pH7) catalysts were almost zero, so they were not listed here. For the catalyst Ni-S15(pH8), the CO conversion and CH<sub>4</sub> yield didn't decline. However, the CH<sub>4</sub> yield of Ni/S15 decreased by 61.2%. Since there were no other side product, the CH<sub>4</sub> yield and CO conversion were equal. Therefore, the Ni-S15(pH8) catalyst had not only a high catalytic activity but also an excellent thermostability.

### 3.2.4 Catalytic stability test

The catalytic stability test of Ni-S15(pH8) and Ni/S15 catalysts were investigated at 400°C under 0.3MPa with a WHSV of 15000 ml/g/h, and the results were shown in Fig.6. The CO conversions of both the catalysts maintained at 100% in the 100h stability test. The CH<sub>4</sub> yields of Ni-S15(pH8) catalyst showed no obvious decrease and maintained at about 95%. However, the CH<sub>4</sub> yields over the Ni/S15 catalyst decreased from 76% to 66% after testing for 100h. Therefore, the Ni-S15(pH8) catalyst showed excellent stability under reaction conditions. It could be seen that the present Ni incorporated SBA-15 catalysts had a good catalytic stability and prospective for the practical application.

As mentioned before, there is a competitive relationship between the CO methanation reaction ( $\text{CO}+3\text{H}_2=\text{CH}_4+\text{H}_2\text{O}$ ) with the WGS reaction ( $\text{CO}+\text{H}_2\text{O}=\text{CO}_2+\text{H}_2$ ) in the process of SNG production. As CO methanation is a structure-insensitive reaction and the water-gas shift reaction is a structure-sensitive reaction [43, 44], the catalytic performance of the catalyst in the methanation process is obviously affected by the metal dispersion and particle size [45]. Zhang et al. [46] found that the relatively larger particle size of metal nickel in the catalyst was conducive to the WGS reaction. For the catalyst Ni/S15, the nickel particles were sintered with time in the stability test due to the weak interaction between nickel and support. Therefore, as the nickel crystalline size increased, CO conversion had no obvious decline but the selectivity of CH<sub>4</sub> and the yield of CH<sub>4</sub> declined. According to the results of TPR, it was considered that stronger interaction between active sites and the SBA-15 support effectively obstructed the sintering of nickel in the syngas methanation reaction. This could ultimately lead to excellent catalytic stability. Combined with the results of H<sub>2</sub> pulse chemisorption, the Ni-S15(pH8) catalyst had the larger surface area and better dispersion of nickel

particles which resulted in more active sites and higher catalytic activity. In conclusion, the excellent catalytic activity and stability could be obtained at the same time for the Ni-S15(pH8) catalyst.

In order to compare the catalytic performance of the Ni-S15 catalyst with the results in the literatures, some syngas methanation catalysts were listed in Tab.4. It should be noted that it was difficult to directly compare the performance of these catalysts because different reaction conditions were used. However, more than 90% of CH<sub>4</sub> selectivity was difficult to reach and some nickel catalysts deactivated rapidly. In consequence, the Ni-S15(pH8) catalyst possessed excellent catalytic performance with good application prospects for the production of SNG.

#### 4. Conclusions

In summary, uniformly dispersed Ni-incorporated SBA-15 materials have been directly synthesized by the pH-adjusting method. The pH of the system was adjusted to a certain value by adding sodium hydroxide aqueous solution. The physicochemical properties of the catalysts were characterized by XRD, N<sub>2</sub> adsorption-desorption, H<sub>2</sub>-TPR, ICP elemental analysis, H<sub>2</sub> pulse chemisorption and TEM. The incorporation of nickel ions was strongly affected by the pH in the synthesis gel. Comparing with the Ni/S15 catalyst, the nickel dispersion and surface area of the catalysts prepared by pH-adjusting method were effectively improved. In addition, Ni-S15 catalyst exhibited much higher activity than Ni/S15 catalyst in CO methanation reaction. The Ni-S15(pH8) catalyst achieved the best activity with 100% CO conversion and about 98.6% CH<sub>4</sub> yield at 350°C, 0.3MPa and 15000mL/g/h. According to the results of TPR analysis, it could be speculated that using

pH-adjusting method could strengthen the interactions between NiO and support. Therefore, Ni-S15 catalyst showed better high-temperature-resistant performance than Ni/S15 catalyst. Meanwhile, it possessed excellent stability in the CO methanation reaction.

## Acknowledgments

This research was financially supported by National Natural Science Funds of China (Grant No. U1203293 and 91434128), the Program of Shanghai Subject Chief Scientist (Grant No. 10XD1401500) and the Program of Shanghai Leading Talents (2013).

## References

- [1] S. P., S.J. B., *Acad. Sci.* (1902) 514-516.
- [2] J. Kopyscinski, T.J. Schildhauer, S.M.A. Biollaz, *Fuel* 89 (2010) 1763-1783.
- [3] S. Li, X.Z. Ji, X.S. Zhang, L. Gao, H.G. Jin, *Applied Energy* 136 (2014) 98-109.
- [4] G.A. Mills, F.W. Steffgen, *Catalysis Reviews* 8 (2006) 159-210.
- [5] A. Zhao, W. Ying, H. Zhang, H. Ma, D. Fang, *Energy Sources, Part A: Recovery, Utilization, and Environmental Effects* 36 (2014) 1049-1056.
- [6] S.L. Ma, Y.S. Tan, Y.Z. Han, *Journal of Natural Gas Chemistry* 20 (2011) 435-440.
- [7] D. Hu, J. Gao, Y. Ping, L. Jia, P. Gunawan, Z. Zhong, G. Xu, F. Gu, F. Su, *Industrial & Engineering Chemistry Research* 51 (2012) 4875-4886.
- [8] X.B. Bai, S. Wang, T.J. Sun, S.D. Wang, *Reaction Kinetics Mechanisms and Catalysis* 112 (2014) 437-451.
- [9] M. Bartolini, J. Molina, J. Alvarez, M. Goldwasser, P.P. Almao, M.J.P. Zurita, *Journal of Power Sources* 285 (2015) 1-11.
- [10] H. Zhang, Y.Y. Dong, W.P. Fang, Y.X. Lian, *Chinese Journal of Catalysis* 34 (2013) 330-335.
- [11] J.Y. Zhang, Z. Xin, X. Meng, Y.H. Lv, M. Tao, *Fuel* 116 (2014) 25-33.
- [12] J.Y. Zhang, Z. Xin, X. Meng, M. Tao, *Fuel* 109 (2013) 693-701.
- [13] D.Y. Zhao, J.Y. Sun, Q.Z. Li, G.D. Stucky, *Chemistry of Materials* 12 (2000) 275.

- [14] C. Tangarnjanavalukul, W. Donphai, T. Witoon, S. Chareonpanich, J. Limtrakul, *Chemical Engineering Journal* 262 (2015) 364-371.
- [15] P. Shah, N. Sridevi, A. Prabhune, V. Ramaswamy, *Microporous and Mesoporous Materials* 116 (2008) 157-165.
- [16] Z.W. Jin, X.D. Wang, X.G. Cui, *Colloids and Surfaces a-Physicochemical and Engineering Aspects* 316 (2008) 27-36.
- [17] J. van der Meer, I. Bardez-Giboire, C. Mercier, B. Revel, A. Davidson, R. Denoyel, *Journal of Physical Chemistry C* 114 (2010) 3507-3515.
- [18] V. Mohan, C.V. Pramod, M. Suresh, K.H.P. Reddy, B.D. Raju, K.S.R. Rao, *Catalysis Communications* 18 (2012) 89-92.
- [19] Q.L. Yao, Z.H. Lu, K.K. Yang, X.S. Chen, M.H. Zhu, *Scientific Reports* 5 (2015).
- [20] J. Taghavimoghaddam, G.P. Knowles, A.L. Chaffee, *Topics in Catalysis* 55 (2012) 571-579.
- [21] Y. Li, W.H. Zhang, L. Zhang, Q.H. Yang, Z.B. Wei, Z.C. Feng, C. Li, *Journal of Physical Chemistry B* 108 (2004) 9739-9744.
- [22] W.H. Zhang, J.Q. Lu, B. Han, M.J. Li, J.H. Xiu, P.L. Ying, C. Li, *Chemistry of Materials* 14 (2002) 3413-3421.
- [23] Y. Li, Z.C. Feng, Y.X. Lian, K.Q. Sun, L. Zhang, G.Q. Jia, Q.H. Yang, C. Li, *Microporous and Mesoporous Materials* 84 (2005) 41-49.
- [24] Z. Lou, R. Wang, H. Sun, Y. Chen, Y. Yang, *Microporous and Mesoporous Materials* 110 (2008) 347-354.
- [25] P. Shah, A.V. Ramaswamy, K. Lazar, V. Ramaswamy, *Microporous and Mesoporous Materials* 100 (2007) 210-226.
- [26] S. Wu, Y. Han, Y.C. Zou, J.W. Song, L. Zhao, Y. Di, S.Z. Liu, F.S. Xiao, *Chemistry of Materials* 16 (2004) 486-492.
- [27] H. Cui, Y. Zhang, Z. Qiu, L. Zhao, Y. Zhu, *Applied Catalysis B: Environmental* 101 (2010) 45-53.
- [28] B. Lu, K. Kawamoto, *RSC Advances* 2 (2012) 6800.
- [29] Z. Xin, M. Tao, patent CN. 2014107241600 (2014).
- [30] N. Wang, W. Chu, T. Zhang, X.S. Zhao, *International Journal of Hydrogen Energy* 37 (2012)

19-30.

- [31] D. Tian, Z. Liu, D. Li, H. Shi, W. Pan, Y. Cheng, *Fuel* 104 (2013) 224-229.
- [32] R. Razzaq, C. Li, M. Usman, K. Suzuki, S. Zhang, *Chemical Engineering Journal* 262 (2015) 1090-1098.
- [33] D. Kim, B.S. Kwak, B.-K. Min, M. Kang, *Applied Surface Science* 332 (2015) 736-746.
- [34] W.H. Zhang, L. Zhang, J.H. Xiu, Z.Q. Shen, Y. Li, P.L. Ying, C. Li, *Microporous and Mesoporous Materials* 89 (2006) 179-185.
- [35] X.A. Diao, Y.J. Wang, J.Q. Zhao, S.L. Zhu, *Chinese Journal of Chemical Engineering* 18 (2010) 493-499.
- [36] D.Y. Han, H.Y. Yang, C.B. Shen, X. Zhou, F.H. Wang, *Powder Technology* 147 (2004) 113-116.
- [37] Y.H. Ikuhara, T. Saito, S. Takahashi, Y. Sasaki, T. Hirayama, T. Gur, *Journal of the American Ceramic Society* 95 (2012) 524-529.
- [38] Y.F. Shao, L.Z. Wang, J.L. Zhang, M. Anpo, *Journal of Physical Chemistry B* 109 (2005) 20835-20841.
- [39] A. Alihosseinzadeh, B. Nematollahi, M. Rezaei, E.N. Lay, *International Journal of Hydrogen Energy* 40 (2015) 1809-1819.
- [40] J. Gao, Q. Liu, F. Gu, B. Liu, Z. Zhong, F. Su, *Rsc Advances* 5 (2015) 22759-22776.
- [41] Z. Liu, B. Chu, X. Zhai, Y. Jin, Y. Cheng, *Fuel* 95 (2012) 599-605.
- [42] S.Y. Chen, C.Y. Tang, J.F. Lee, L.Y. Jang, T. Tatsumi, S. Cheng, *Journal of Materials Chemistry* 21 (2011) 2255-2265.
- [43] X.Z. Yang, W. Wendurima, G.J. Gao, Q.Q. Shi, X. Wang, J.A. Zhang, C.H. Han, J. Wang, H.L. Lu, J. Liu, M. Tong, *International Journal of Hydrogen Energy* 39 (2014) 3231-3242.
- [44] S. Velu, S. Gangwal, *Solid State Ionics* 177 (2006) 803-811.
- [45] C.M. Jia, J.J. Gao, J. Li, F.N. Gu, G.W. Xu, Z.Y. Zhong, F.B. Su, *Catalysis Science & Technology* 3 (2013) 490-499.
- [46] G.Q. Zhang, T.J. Sun, J.X. Peng, S. Wang, S.D. Wang, *Applied Catalysis a-General* 462 (2013) 75-81.
- [47] J.J. Gao, C.M. Jia, M.J. Zhang, F.N. Gu, G.W. Xu, F.B. Su, *Catalysis Science & Technology* 3 (2013) 2009-2015.

- [48] J. Li, L. Zhou, P.C. Li, Q.S. Zhu, J.J. Gao, F.N. Gu, F.B. Su, *Chemical Engineering Journal* 219 (2013) 183-189.
- [49] X. Chen, J. Jin, G. Sha, C. Li, B. Zhang, D. Su, C.T. Williams, C. Liang, *Catalysis Science & Technology* 4 (2014) 53.

**Figure captions**

Figure 1 XRD patterns of Ni-based catalysts. (A) Small angle XRD patterns (B) wide angle XRD patterns.

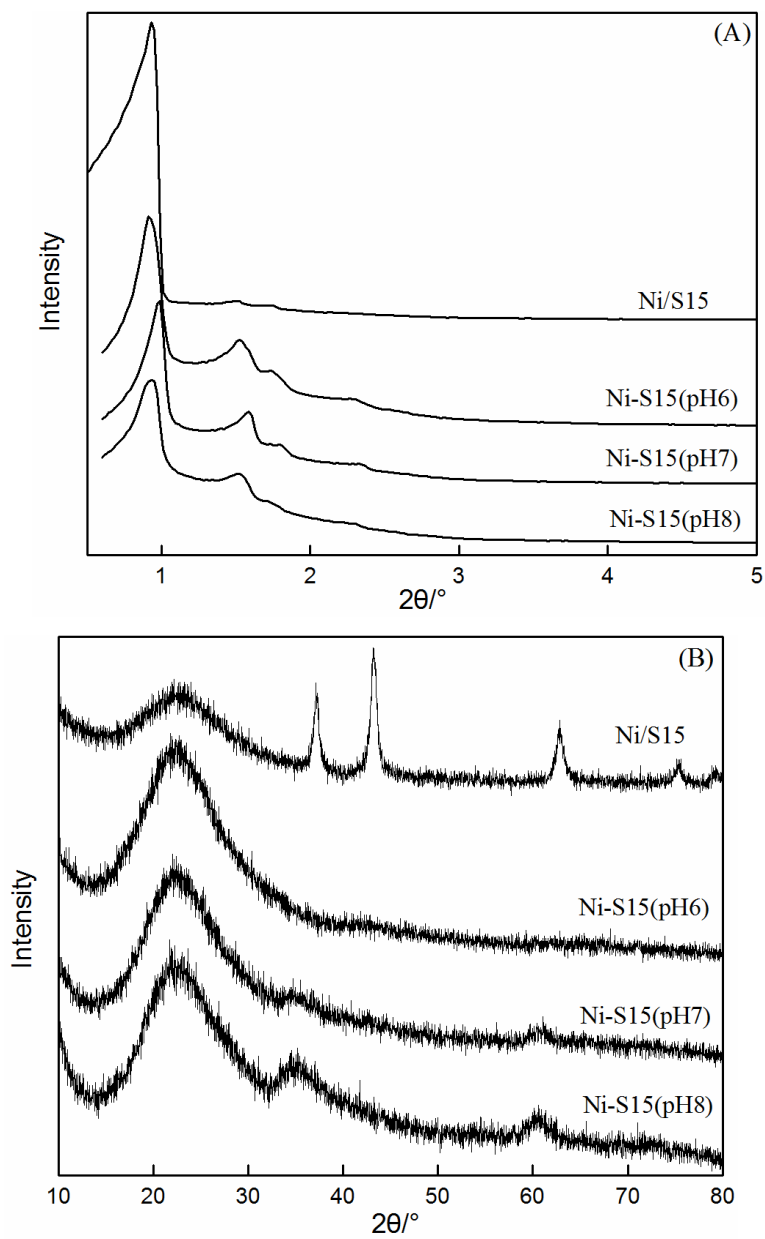


Figure 2 SEM of SBA-15 (A) and TEM-EDS images of Ni-based catalysts. (B) SBA-15, (C) Ni-S15(pH6), (D) Ni-S15(pH7), (E) Ni-S15(pH8), (F) Ni/S15.

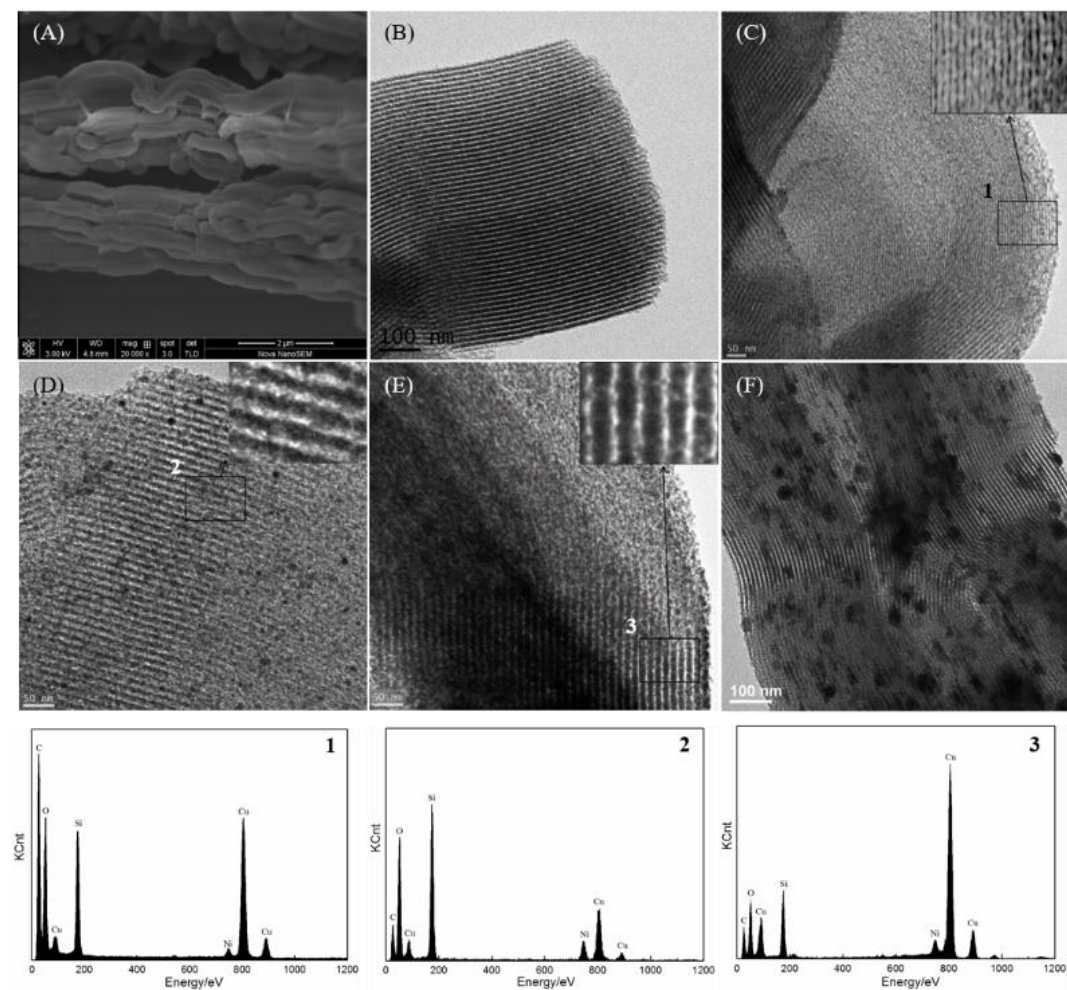


Figure 3 A schematic diagram for the preparation of the Ni incorporated SBA-15 catalyst.

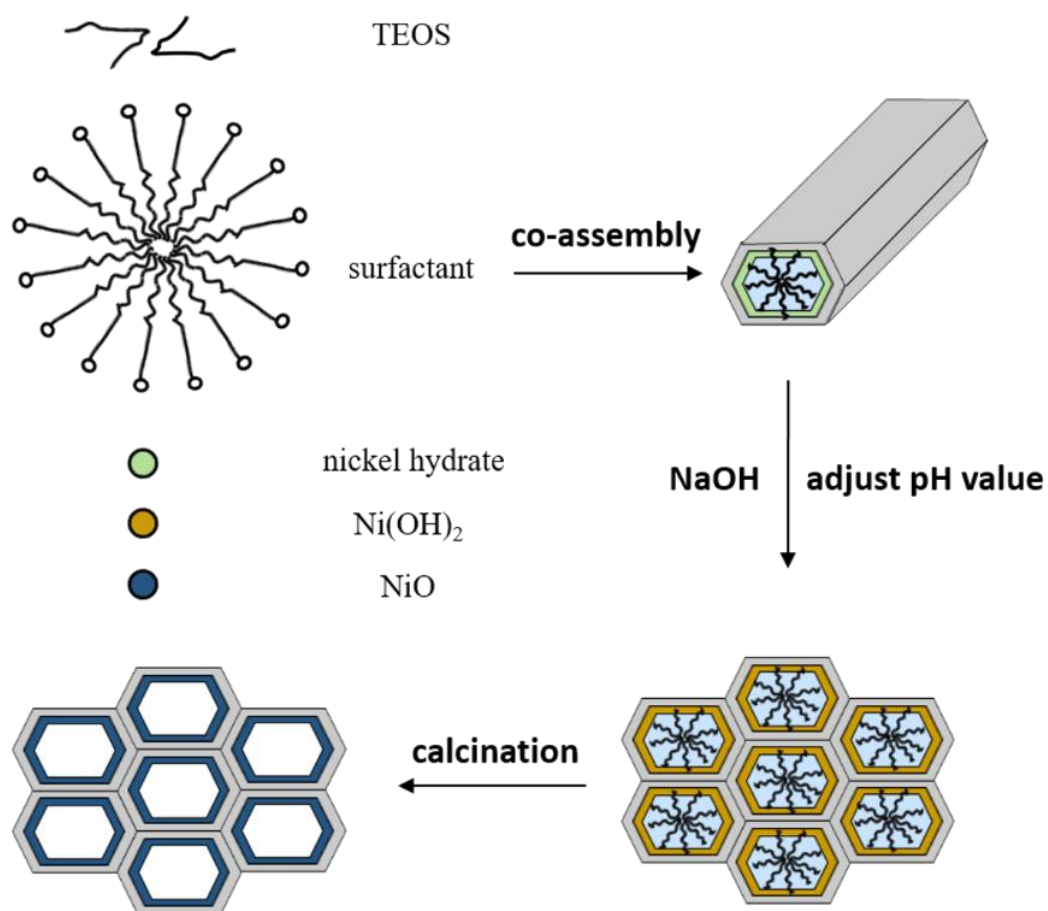


Figure 4 TPR profiles of Ni-based SBA-15 catalysts.

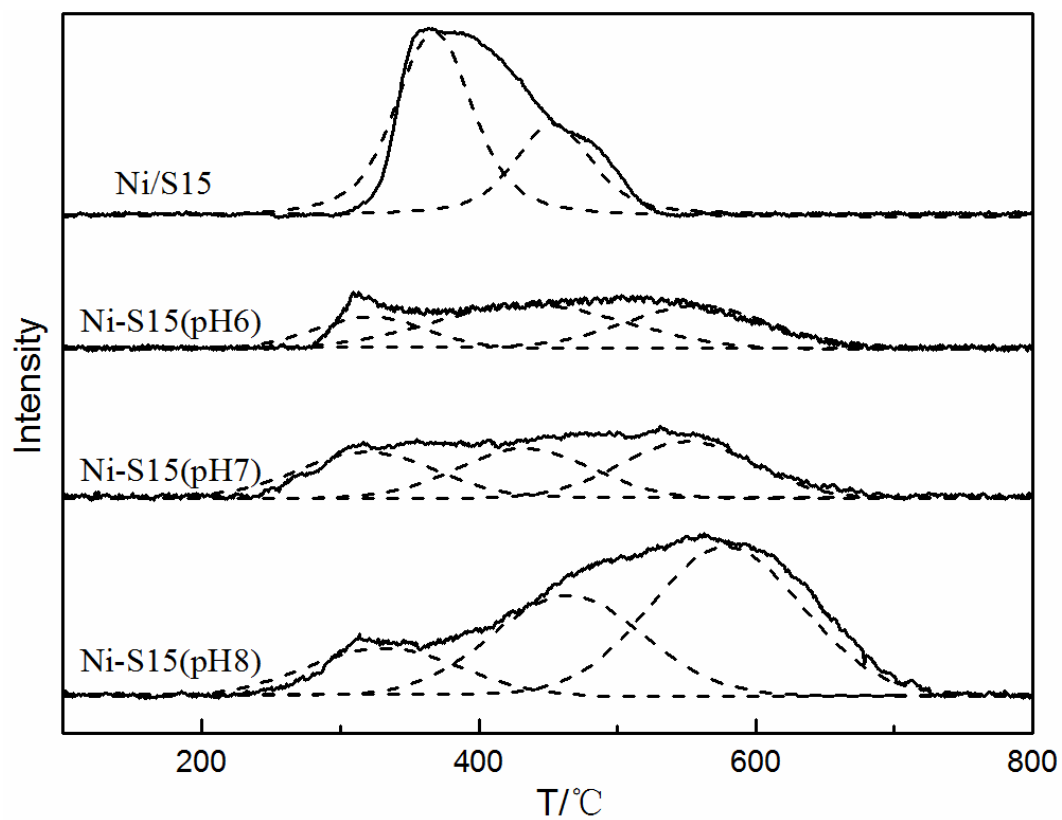


Figure 5 Effect of pH value on the catalytic performance of the catalysts. (A) CO conversion, (B)CH<sub>4</sub> yield. Condition: n(H<sub>2</sub>):n(CO) =3:1, 15000 ml/g/h, 0.3MPa.

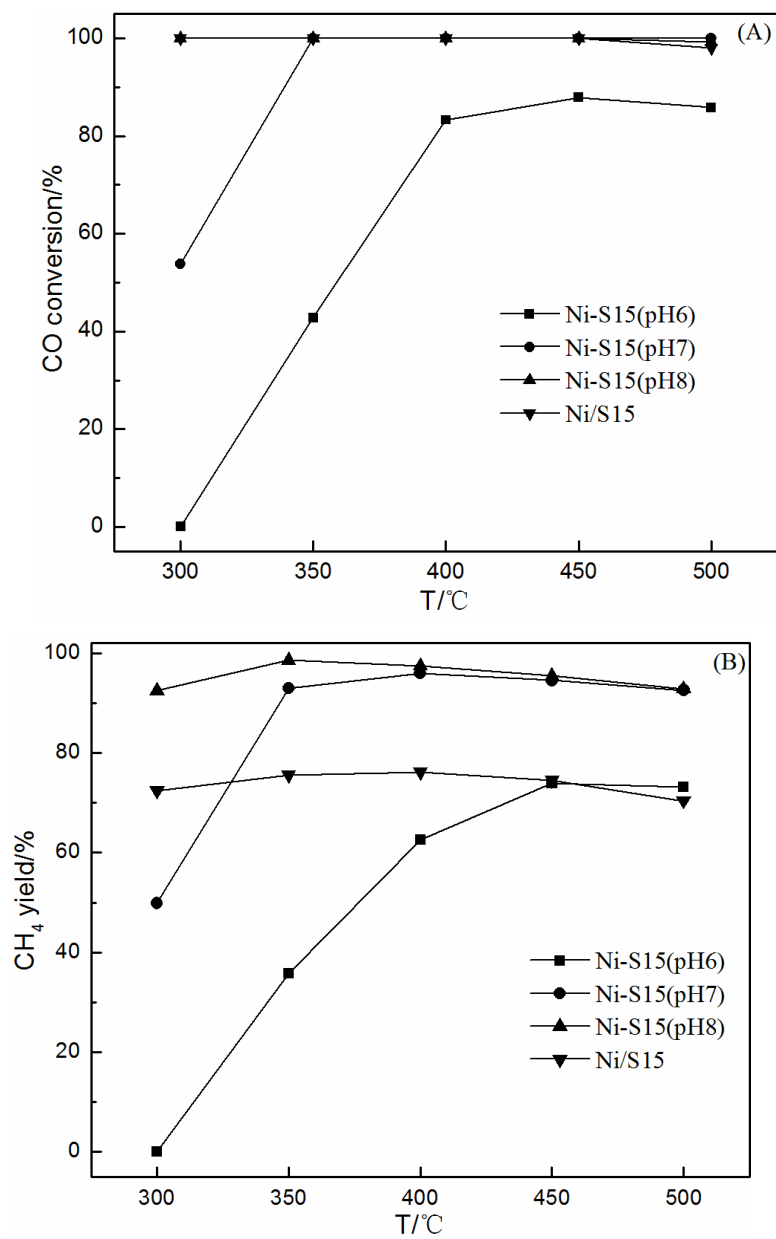
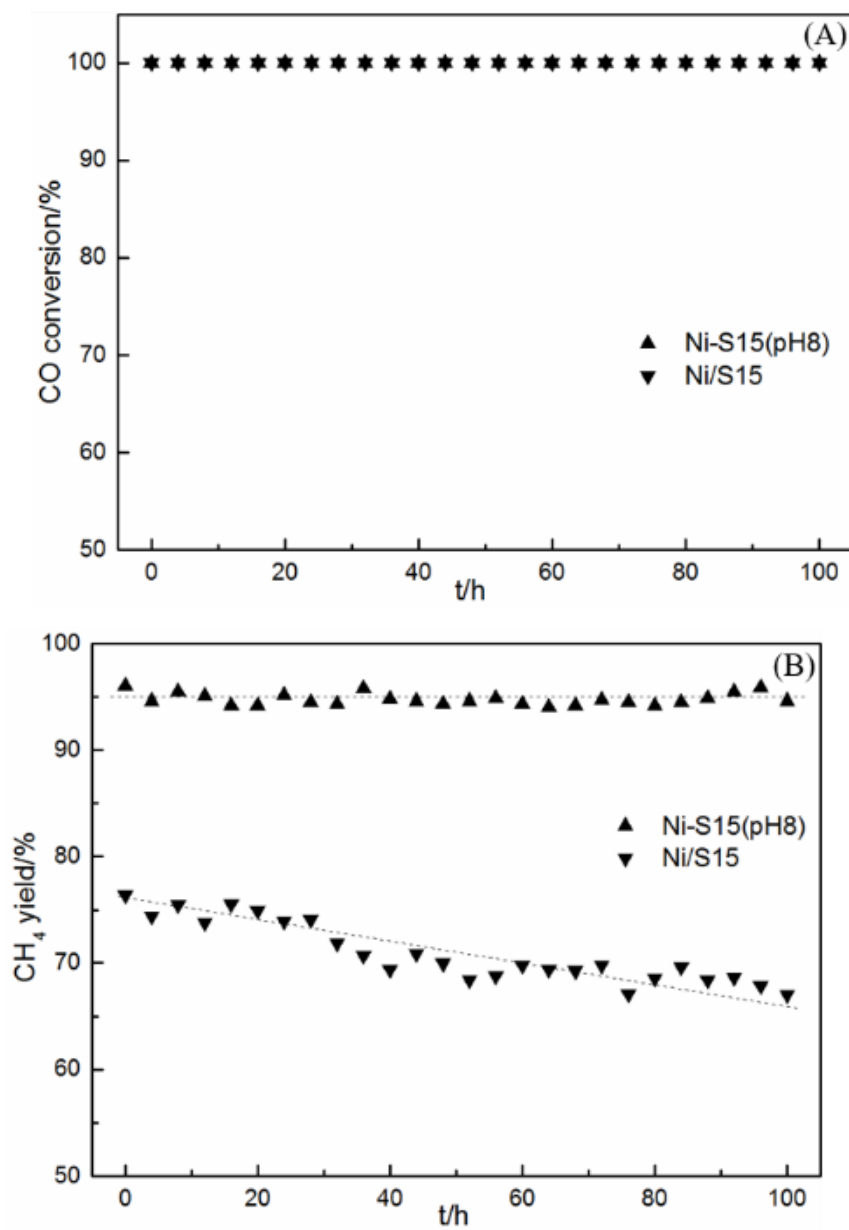


Figure 6 Catalytic stability of the Ni-S15(pH8) and Ni/S15 catalysts. (A) CO conversion, (B) CH<sub>4</sub> yield. Condition: n(H<sub>2</sub>):n(CO) = 3:1, 15000 ml/g/h, 400 °C, 0.3MPa.



## Table captions

Table1 Physicochemical properties of SBA-15 and catalysts.

Samples	BET surface area <sup>a</sup> (m <sup>2</sup> /g)	Average pore size <sup>b</sup> (nm)	BET surface area <sup>c</sup> (m <sup>2</sup> /g)	Average pore size <sup>d</sup> (nm)	Nickel content <sup>e</sup> (wt%)	Metal dispersion <sup>f</sup> (%)	Metallic surface area <sup>f</sup> (m <sup>2</sup> /g)	Metal dispersion <sup>g</sup> (%)
SBA-15	756	5.1	400	3.9	-	-	-	-
Ni-S15(pH6)	620	7.9	502	7.8	1.7	2.0	0.8	1.1
Ni-S15(pH7)	600	8.3	483	8.3	5.4	2.8	1.6	2.2
Ni-S15(pH8)	422	9.8	326	9.6	8.4	3.6	2.0	3.5
Ni/S15	476	6.1	358	5.8	9.8	2.5	1.1	1.4

a Calculated by the BET equation.

b BJH desorption average pore size.

c BET surface area of the catalyst calcined in feed gas at 700°C for 2h and calculated by the BET equation.

d BJH desorption average pore size of the catalyst calcined in feed gas at 700°C for 2h.

e Calculated by ICP-AES.

f Calculated by H<sub>2</sub> pulse chemisorption.

g Metal dispersion of the catalyst calcined in feed gas at 700°C for 2h and calculated by H<sub>2</sub> pulse chemisorption.

Table 2 TPR quantitative data of the catalysts.

Catalyst	Tm(°C)			Fraction of total area (%)		
	I	II	III	I	II	III
Ni/S15	366.7	454.6	-	0.68	0.32	-
Ni-S15(pH6)	327.3	437.5	539.0	0.34	0.34	0.32
Ni-S15(pH7)	320.4	432.7	551.2	0.19	0.48	0.33
Ni-S15(pH8)	332.5	464.5	579.1	0.16	0.34	0.50

Table 3 Thermostability performance of Ni-based catalysts.

Catalysts	Reaction temperature/ °C	Before Calcination		After Calcination	
		CH <sub>4</sub> yield /%	CO conversion/%	CH <sub>4</sub> yield /%	CO conversion/%
Ni-S15(pH6)	400	62.6	83.3	39.1	61.6
Ni-S15(pH7)	400	96.0	100	79.8	96.3
Ni-S15(pH8)	400	97.5	100	97.4	100
	250	64.2	64.2	63.8	63.8
Ni/S15	400	76.2	100	45.7	67.5
	250	39.7	39.7	15.4	15.4

Table 4 Summary of the syngas methanation catalysts developed in recent years.

Catalysts	Preparation methods	Active metal content wt%	Catalytic performance					Stability test time/h	Reference
			P/MPa	WHSV /( $\text{mL} \cdot \text{g}^{-1} \cdot \text{h}^{-1}$ )	T/°C	X <sub>CO</sub> /%	S <sub>CH<sub>4</sub></sub> /%		
Ni-Al <sub>2</sub> O <sub>3</sub>	CP	15	0.1	2500 h <sup>-1</sup>	400	98.2	84.7	120*	[6]
Ni-Al <sub>2</sub> O <sub>3</sub>	I	10	0.1	240 000	450	61	68	50*	[47]
Ni-Mg-Al <sub>2</sub> O <sub>3</sub>	I	40	0.1	36 000	300	64	58	50	[48]
Si-Ni/SiO <sub>2</sub>	Silicification	20	0.1	4800	350	50	28	42	[49]

Ni/MCM-4 1	HT	10	0.1	12 000	350	97.9	88.2	100	[12]
Ni/CaTiO <sub>3</sub>	I	10	3.0	10 000	350	95	72	50	[45]

I: impregnation; CP: co-precipitation; HT: hydrothermal synthesis; \* deactivation was observed.